Fundamental Properties of the Field at the Interface Between Air and a Periodic Artificial Material Excited by a Line Source

Filippo Capolino, *Senior Member, IEEE*, David R. Jackson, *Fellow, IEEE*, and Donald R. Wilton, *Fellow, IEEE*

***Abstract*—An efficient algorithm based on a moment-method formulation is presented for the evaluation of the field produced by a line source at the interface between an air superstrate and a one-dimensional-periodic artificial-material slab. The formulation provides physical insight into the nature of the fields via path deformation in the complex wavenumber plane. From an asymptotic analysis in the complex wavenumber plane it is found that the space wave produced by a line source consists of an infinite number of space harmonics that decay algebraically as $x^{-3/2}$. Guided modes may also exist and be excited, including leaky modes.**

***Index Terms*—Artificial surfaces, electromagnetic bandgap (EBG), metamaterials, periodic structures, photonic bandgap (PBG).**

I. Introduction

PERIODIC artificial surfaces and materials such as electromagnetic bandgap (EBG) structures [1], artificial magnetic conductors [2] and artificially soft surfaces [3] have been used recently to modify the radiation pattern and other characteristics of sources located near or within them. For example, artificial EBG materials have been used to suppress surface-wave propagation on dielectric substrates [2], [4], [5]. Artificial surfaces and materials have also been used to obtain highly directive antenna patterns in the microwave and millimeter-wave ranges [6], [7]. Artificially soft surfaces have found use in several fields, including applications that require the attenuation of the spatial field produced by a source along an interface [8].

In the present investigation an efficient numerical scheme for evaluating the field produced by a line source above an artificial material (or any other periodic structure) that is periodic in one-dimension (1-D) is first examined. For simplicity, a two-dimensional (2-D) problem is considered (see Fig. 1), which is invariant along the y dimension, with a 1-D-periodicity along x (in the following, a material periodic in one dimension is called 1-D-periodic material.) An extension of the method to 2-D-periodic structures, periodic along x and y, is possible, but is not considered here. The focus is then placed on some fundamental properties pertaining to the nature of the field along the interface between air and the material. The results are directly applicable to determining the coupling between sources located in proximity of a periodic artificial structure, such as a wire medium of finite thickness.

The periodic artificial material consists of a periodic (along x) structure made of layers of conducting strips or cylinders, with period a. A finite number of layers may be stacked along z to form an artificial material slab with a finite thickness as shown in Fig. 1(a), or there may be a single layer of elements, as for the corrugated structure of Fig. 1(b) or the strip grating of Fig. 1(c). An electric line source in the y direction (parallel to the periodic elements) is either placed inside or outside the artificial material, at (x_0, z_0). (The method could be extended to treat the case of a dipole excitation near the 1-D periodic structure, but this is not considered here.) The problem is thus one of transverse electric (TE) (to z) polarization. Although transverse magnetic (TM) polarization could be treated in a similar fashion, the TE case has been selected here for two reasons: first, for consistency with the EBG material consisting of the wire medium in Fig. 1(a), since the TE polarization is most affected by the presence of the wires. Second, to numerically isolate and study the space wave fields on the structure, which is easier in the absence of guided modes. Indeed, as shown in [9], for TM polarization, periodic structures such as the corrugated structure have propagating modes for low frequencies since the structure behaves as an inductive surface, with mode suppression occurring when the depth of the teeth is approximately a quarter wavelength (the structure acts as an artificially soft surface at this point). For the TE case it is possible to obtain a modeless structure, so that the total field excited by the source is the same as the spatial (space-wave) field.

An efficient field evaluation is obtained in Sections II and III using the "array scanning method" [10]–[12]. To improve the computational efficiency of the method, a 2-D Ewald acceleration scheme [13], [14] is used to improve the convergence of the periodic free-space Green's function. The resulting field from the line source then has a representation in the form of an integral in k_x (over the Brillouin zone).

In Section IV an alternative representation of the field from the line source is obtained by "unfolding" the integration over the Brillouin zone onto the entire real axis in the k_x plane. This allows for a convenient path deformation to enclose any singularities in the complex wavenumber plane, including pole and branch-point singularities. In Section V it is shown how the complex wavenumber plane for such problems has an infinite number of periodically spaced branch points, and also a periodic set of poles (assuming that a guided mode exists). (This was anticipated in [15] and demonstrated in [16] for a specific type

Manuscript received February 15, 2004; revised July 1, 2004.

F. Capolino is with the Department of Information Engineering, University of Siena, 53100 Siena, Italy (e-mail: capolino@dii.unisi.it).

D. R. Jackson and D. R. Wilton are with the Department of Electrical and Computer Engineering, University of Houston, Houston, TX 77204-4005 USA (e-mail: djackson@uh.edu).

Digital Object Identifier 10.1109/TAP.2004.840518

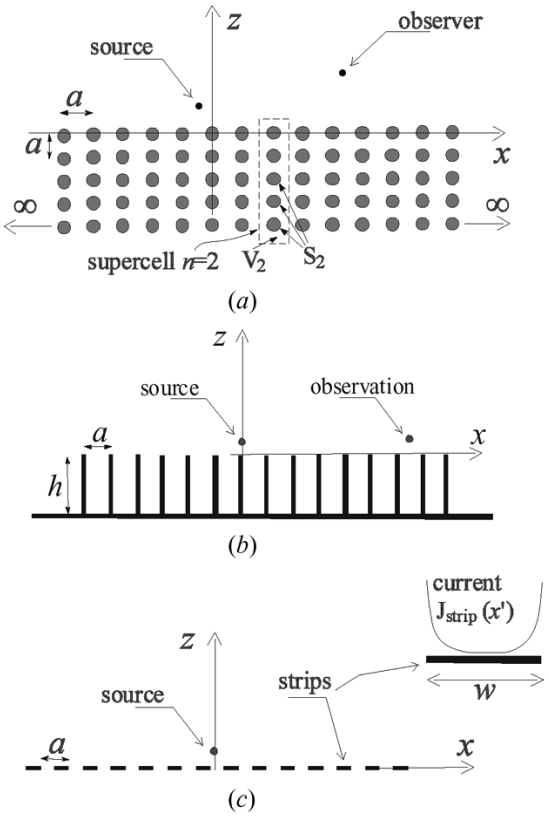

Fig. 1. Geometry of several periodic materials, showing a line-source excitation. In all cases, a denotes the periodicity along x. (a) The material is an infinite periodic array of metallic cylinders with period a that is truncated in the negative z direction after a finite number of layers. In the figure, the periodic supercell (i.e., unit cell with multiple conductors) $n = 2$ is highlighted. The source is located in the $n = 0$ supercell [arrows point to three of the conductors within the $n = 2$ supercell in Fig. 1(a)]. S_n denotes the surface of the conductors in the nth supercell. The volumetric region of the nth supercell is denoted by V_n. (b) A corrugated surface consisting of metallic teeth above a ground plane. The thickness of the teeth is h. (c) A metallic strip grating. Also shown is an expanded view of one of the strips, with a sketch of the current shape for a small strip width w.

of structure. An infinite number of periodically spaced branch points has also been found in a similar problem [17] where the waves arising at the truncation of a periodic set of metallic strips have been rigorously analyzed.) The residue evaluations at the set of poles yields the modal amplitudes of the Floquet harmonics of the guided mode (if any) on the periodic structure, while the branch points determine the space-wave field radiated by the line source. In Section VI a structure consisting of a periodic arrangement of metallic strips is used as an example, since closed-form expressions for the integrand are available in the case of narrow strips. Asymptotic evaluations involving path deformations into steepest-descent paths are used to determine the field behavior on the interface ($z \approx 0$) with increasing distance from the source. In Section VII, it is shown that the general conclusions are valid for a line-source excitation of any artificial material structure comprising a periodic arrangement of conducting objects that are invariant in the y direction, the structure being infinite and periodic in the x direction with a finite extent in the z direction. In Section VIII, results are presented for the structures of Fig. 1 to confirm the validity of the conclusions.

II. The Array Scanning Method

The array scanning method (ASM) (as the method was called in [11], though it had seen previous use, e.g., in [12]) is an analytic procedure that synthesizes the field from a single source in terms of a spectral wavenumber integration over a phased array of sources, as shown in Fig. 2. Therefore, a convenient numerical evaluation of the aperiodic (single source) excitation of an infinite periodic structure such as the EBG material slab in Fig. 1 can be obtained using the ASM. The first step is to note the following relation between an infinite periodic array of impressed linearly-phased line sources $J^{i,\infty}(\mathbf{r}', k_x)$ with currents directed along y, and the corresponding single line source $J^i(\mathbf{r}')$

$$J^{i,\infty}(\mathbf{r}', k_x) = \sum_{m=-\infty}^{\infty} \delta(x' - x_0 - ma)\delta(z' - z_0)e^{-jk_x ma}$$

$$J^i(\mathbf{r}') = \frac{a}{2\pi} \int_{-\pi/a}^{\pi/a} J^{i,\infty}(\mathbf{r}', k_x)\, dk_x \tag{1}$$

where k_x is an impressed wavenumber along x. The single line source $J^i(\mathbf{r}')$ is thus synthesized from the periodic phased array of line sources spaced along the x axis by integrating in the wavenumber variable k_x over the Brillouin zone. The electric field at any point $\mathbf{r}$ produced by the periodic array of phased line sources in free space (the field that is incident on the periodic structure from the phased array of sources) is denoted as

$$E^{\infty}_{\text{inc}}(\mathbf{r}, \mathbf{r}_0, k_x) = -j\omega\mu G^{\infty}(\mathbf{r}, \mathbf{r}_0, k_x), \tag{2}$$

where

$$G^{\infty}(\mathbf{r}, \mathbf{r}_0, k_x) = \frac{1}{2ja} \sum_{p=-\infty}^{\infty} \frac{e^{-j[(x-x_0)k_{xp} + |z-z_0|k_{zp}]}}{k_{zp}} \tag{3}$$

is the periodic Green function for the magnetic vector potential component A_y produced by the phased array of line sources, in which

$$k_{xp} = k_x + \frac{2\pi p}{a} \quad \text{and} \quad k_{zp} = \sqrt{k^2 - k_{xp}^2} \tag{4}$$

are the Floquet mode wavenumbers along x and z, respectively, with k the homogeneous-space ambient wavenumber. There are an infinite number of branch points in the k_x plane, located at

$$k_{b,p}^{\pm} = \pm k - 2\pi p/a. \tag{5}$$

The pth branch point corresponds to the square root involved in k_{zp} that appears in G^{∞}. The top Riemann sheet of the k_x plane for the branch point $k_{b,p}$ is defined as $\Im m(k_{zp}) < 0$. The field produced by the periodic phased array of line sources near the EBG slab is denoted as $E^{\infty}_{\text{tot}}(\mathbf{r}, \mathbf{r}_0, k_x)$. By the same weighted superposition used in (1), the electric field produced by the single source $J^i(\mathbf{r}')$ in that periodic environment is then given by

$$E_{\text{tot}}(\mathbf{r}, \mathbf{r}_0) = \frac{a}{2\pi} \int_{-\pi/a}^{\pi/a} E^{\infty}_{\text{tot}}(\mathbf{r}, \mathbf{r}_0, k_x)\, dk_x. \tag{6}$$

The calculation of $E^{\infty}_{\text{tot}}(\mathbf{r}, \mathbf{r}_0, k_x)$, which involves the periodic moment method, is discussed in the next section.

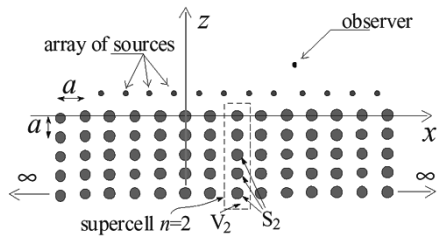

Fig. 2. Illustration of the array scanning method (ASM). The field produced by a single line source is reconstructed from the field produced by an array of sources having the same periodicity as the artificial material.

III. Field Produced by a Line-Source Above a Periodic Material

The electric field in Fig. 1 is polarized along the y direction, since there is no variation along the y axis. For simplicity, we consider here only metallic scatterers, e.g., as those shown in Fig. 1. We denote by $J_S(\mathbf{r})$ and $E(\mathbf{r})$ the surface current in the y direction on the metallic conductors and the electric field directed along y at any point, respectively.

The current $J^{\infty}_{S,\mathrm{post}}$ on the surface of the conductors (posts) within the $n = 0$ supercell due to the phased array of line sources is found by solving the EFIE

$$\int_{S_0} J^{\infty}_{S,\mathrm{post}}(\mathbf{r}',\mathbf{r}_0,k_x)G^{\infty}(\mathbf{r},\mathbf{r}',k_x)\,d\mathbf{r}' = -G^{\infty}(\mathbf{r},\mathbf{r}_0,k_x) \tag{7}$$

for $\mathbf{r} = S_0$, where the periodic Green's function $G^{\infty}(\mathbf{r},\mathbf{r}_0,k_x)$ is accelerated using the 2-D Ewald method [2], [4]. Note that $J^{\infty}_{S,\mathrm{post}}(\mathbf{r}',\mathbf{r}_0,k_x)$ is a periodic function of k_x with period $2\pi/a$. The electric field that is scattered by the periodic structure from the phased array of line sources is determined by integrating over the post currents $J^{\infty}_{S,\mathrm{post}}$ as

$$E^{\infty}_{\mathrm{sca}}(\mathbf{r},\mathbf{r}_0,k_x) = -j\omega\mu\int_{S_0} J^{\infty}_{S,\mathrm{post}}(\mathbf{r}',\mathbf{r}_0,k_x)G^{\infty}(\mathbf{r},\mathbf{r}',k_x)\,d\mathbf{r}' \tag{8}$$

with the integral performed over the post currents within the unit supercell S_0 by using the periodic Green's function $G^{\infty}(\mathbf{r},\mathbf{r}',k_x)$. Note that $E^{\infty}_{\mathrm{sca}}(\mathbf{r},\mathbf{r}_0,k_x)$ is also a periodic function of k_x with period $2\pi/a$. The scattered field in the nth supercell from the single line source is then found from the field within the zeroth supercell in the phased-array problem as

$$E_{\mathrm{sca}}(\mathbf{r}+na\hat{\mathbf{x}},\mathbf{r}_0) = \frac{a}{2\pi}\int_{-\pi/a}^{\pi/a} E^{\infty}_{\mathrm{sca}}(\mathbf{r},\mathbf{r}_0,k_x)e^{-jk_xna}\,dk_x \tag{9}$$

where $\mathbf{r}\in V_0$. The total field is obtained by adding the scattered field (9) to the incident field produced by the line source,

$$E_{\mathrm{tot}} = E_{\mathrm{sca}} + E_{\mathrm{inc}}. \tag{10}$$

It has been observed that the integrand $E^{\infty}_{\mathrm{sca}}$ in (9) has a branch point singular behavior at $k_x = \pm k$ that may result in a numerical inefficiency in the numerical integration of (9). (There are an infinite number of branch points, as seen from (5), although only these two branch points are encountered for many practical situations, where $ka < \pi$.) To overcome this difficulty, the total electric field E_{tot} in (10) could alternatively be obtained by representing the incident electric field in terms of its spectral representation

$$E_{\mathrm{inc}}(\mathbf{r}+na\hat{\mathbf{x}},\mathbf{r}_0) = \frac{a}{2\pi}\int_{-\pi/a}^{\pi/a} E^{\infty}_{\mathrm{inc}}(\mathbf{r},\mathbf{r}_0,k_x)e^{-jk_xna}\,dk_x. \tag{11}$$

with $E^{\infty}_{\mathrm{inc}}$ given in (2). The total electric field (10) is thus expressed as

$$E_{\mathrm{tot}}(\mathbf{r}+na\hat{\mathbf{x}},\mathbf{r}_0) = \frac{a}{2\pi}\int_{-\pi/a}^{\pi/a} E^{\infty}_{\mathrm{tot}}(\mathbf{r},\mathbf{r}_0,k_x)e^{-jk_xna}\,dk_x \tag{12}$$

where

$$E^{\infty}_{\mathrm{tot}}(\mathbf{r},\mathbf{r}_0,k_x) = E^{\infty}_{\mathrm{sca}}(\mathbf{r},\mathbf{r}_0,k_x) + E^{\infty}_{\mathrm{inc}}(\mathbf{r},\mathbf{r}_0,k_x). \tag{13}$$

While the integrand $E^{\infty}_{\mathrm{sca}}$ in (9) at $k_x = \pm k$ possesses a singularity behavior of the type $1/\sqrt{k^2-k_x^2}$, the integrand $E^{\infty}_{\mathrm{tot}}$ in (12) instead contains weaker branch point singularities of the type $A+\sqrt{k^2-k_x^2}$. (Physically, this corresponds to the fact that the total spatial field along the interface decays faster than does the scattered field alone.) These features are established in Appendix A and Section VII. Because the integrand in (12) is less singular than that in (9), the integration requires fewer-integration points near the branch point singularities at $k_x = \pm k$.

IV. Unfolding the Integration Path

The integrand in (9) is a periodic function of k_x with period $2\pi/a$. Indeed, $E^{\infty}_{\mathrm{sca}}(\mathbf{r},\mathbf{r}_0,k_x)$ is periodic because $J^{\infty}_{S,\mathrm{post}}(\mathbf{r}',\mathbf{r}_0,k_x)$ is excited by a periodic (in k_x) phased array of line sources. After inserting (8) into (9), and using the explicit form of the Green's function in (3), (8) is written as

$$\begin{aligned} &E_{\mathrm{sca}}(\mathbf{r}+na\hat{\mathbf{x}},\mathbf{r}_0)\\ &\quad= \frac{-\omega\mu}{4\pi}\int_{S_0}\int_{-\pi/a}^{\pi/a}\sum_{p=-\infty}^{\infty}\frac{\mathrm{e}^{-j[(x+na-x')k_{xp}+|z-z'|k_{zp}]}}{k_{zp}}\\ &\qquad\times J^{\infty}_{S,\mathrm{post}}(\mathbf{r}',\mathbf{r}_0,k_x)\,dk_x\,d\mathbf{r}'. \end{aligned} \tag{14}$$

Since the term $J^{\infty}_{S,\mathrm{post}}(\mathbf{r}',\mathbf{r}_0,k_x)$ is periodic in k_x, applying the shift of variables $k_x+2\pi p/a \to k_x$ for every p term of the sum leads to

$$\begin{aligned} &E_{\mathrm{sca}}(\mathbf{r}+na\hat{\mathbf{x}},\mathbf{r}_0)\\ &\quad= \frac{-\omega\mu}{4\pi}\int_{S_0}\int_{-\infty}^{\infty}\frac{\mathrm{e}^{-j[(x+na-x')k_x+|z-z'|k_z]}}{k_z}\\ &\qquad\times J^{\infty}_{S,\mathrm{post}}(\mathbf{r}',\mathbf{r}_0,k_x)\,dk_x\,d\mathbf{r}' \end{aligned} \tag{15}$$

which eliminates the sum and expresses the scattered field as a continuous integration over the entire k_x axis, physically corresponding to a continuous-spectrum plane wave expansion of the scattered field.

V. The Complex k_x Plane and Field Representation

In addition to the two branch-point singularities introduced by the k_z term in (15), the periodic function $J^{\infty}_{S,\mathrm{post}}(\mathbf{r}', \mathbf{r}_0, k_x)$ introduces a periodic set of branch-point singularities. Furthermore, this function may also exhibit a periodic set of poles, each one representing modal propagation along x. The branch point singularities at $k^{\pm}_{b,p}$ in (5) of the spectral function $J^{\infty}_{S,\mathrm{post}}(\mathbf{r}', \mathbf{r}_0, k_x)$ arise from the periodic Green's function in (7) and are shown in Fig. 3. This figure also shows a possible set of periodic pole singularities, representing a leaky mode on the structure (with a complex wavenumber). Complex poles are located symmetrically with respect to both the real and imaginary axes, though only one set of poles is shown here for simplicity (the set that is shown corresponds to a physical leaky mode in the fourth quadrant of the fundamental Brillouin zone). If the mode is a physical leaky mode radiating in the forward direction, then it is on the improper sheet with respect to its nearest branch point, and on the top sheet of all other branch points. This corresponds to a mode for which all of the space harmonics (Floquet waves) of the guided mode on the structure are proper (decaying vertically) except for the one that is a fast wave, i.e., that with wavenumber smaller than k. If the mode is a physical leaky mode radiating into the backward region, then all of the poles are on the top sheet of all the branch points. (In this case the pole located in the fundamental Brillouin zone would have a negative phase constant.)

As shown in Fig. 3, the original integration path on the real axis can be deformed around the spectral singular points to highlight the space-wave and modal contributions. When evaluating the total field, the path deformation leads to the representation

$$E_{\mathrm{tot}}(\mathbf{r}, \mathbf{r}_0) = E_{\mathrm{mode}}(\mathbf{r}, \mathbf{r}_0) + E_{\mathrm{sp}}(\mathbf{r}, \mathbf{r}_0) \tag{16}$$

where the modal field E_{mode} arises from the reside evaluations at the periodic pole locations, with the residue at each location determining the amplitude of the corresponding Floquet mode contribution to the guided leaky mode. The space-wave field E_{sp} arises from the evaluation of the integral around each branch point.

In the case of $|z-z'| \ll |x+na-x'|$, the vertical paths shown in the figure are the steepest descent paths. One can infer that the space wave arises from all of the branch points, and consists of an infinite number of space harmonics.

From an asymptotic evaluation of the spectral integral carried out in Appendix B, it is seen that each space harmonic that is part of the space-wave field has a spreading factor $1/(x)^{3/2}$ along the interface. The remaining spatial integral in (15) determines the weight of each decaying spatial harmonic.

VI. Canonical Example: Strip Grating in Free Space

Some properties derived from the above discussion are illustrated for the simple case of a single-layer periodic structure consisting of an infinite periodic arrangement of narrow conducting strips located at $z = 0$ and excited by an electric line source at $(x_0, z_0) = (0, z_0)$. We assume a fixed current distribution on each strip, proportional to the basis function $J_{\mathrm{strip}}(x') = 1/[\pi\sqrt{1-(2x'/w)^2}]$ defined about the center of each strip. This is a good approximation when $w \ll \lambda$, with

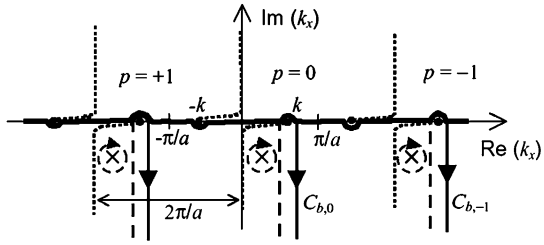

Fig. 3. Spectral k_x plane. The poles and branch points are periodic in the k_x plane, with period $2\pi/a$. The original path on the real axis (detouring around the branch-point singularities) is shown, along with the path deformation around the periodically spaced branch points and leaky-wave poles.

λ the free-space wavelength. This simple case allows for an analytic solution for the strip current in the 0th unit cell when the structure is illuminated by the phased array of line sources, as

$$J^{\infty}_{S,\mathrm{strip}}(x', k_x) = I(k_x) J_{\mathrm{strip}}(x') \tag{17}$$

with

$$I(k_x) = -\frac{\sum_{p=-\infty}^{\infty} \frac{\exp(jk_{zp}z_0)}{k_{zp}} J_0(k_{xp}w/2)}{\sum_{p=-\infty}^{\infty} \frac{1}{k_{zp}} J_0^2(k_{xp}w/2)} \tag{18}$$

where the Bessel function of zeroth order, $J_0(k_x w/2)$, is the Fourier transform of the basis function. From this current representation it is immediate to see that the infinite periodic arrangement of branch points is as shown in Fig. 3. The expression for the scattered field in (15) is represented as

$$E_{\mathrm{sca}}(\mathbf{r} + na\hat{\mathbf{x}}, \mathbf{r}_0) = \frac{-\omega\mu}{4\pi} \int_{-\infty}^{\infty} \frac{\mathrm{e}^{-j(x+na)k_x - j|z|k_z}}{k_z} \tilde{J}_0^{\infty}(k_x)\, dk_x \tag{19}$$

with

$$\begin{aligned} \tilde{J}_0^{\infty}(k_x) &= \int_{-w/2}^{w/2} \mathrm{e}^{+jx'k_x} J^{\infty}_{S,\mathrm{strip}}(x', k_x)\, dx' \\ &= I(k_x) J_0(k_x w/2). \end{aligned} \tag{20}$$

It can be shown (see also the general discussion in Section VII) that near the branch point at $k_x = k, k_z \approx 0$ and the current function $\tilde{J}_0^{\infty}(k_x)$ in (20) behaves as

$$\tilde{J}_0^{\infty}(k_x) \approx -1 + A_0 k_z + B_0 k_z^2. \tag{21}$$

As detailed in Appendix B, the dominant term arising from the constant -1 at the branch $k_x = k$ yields the field

$$\begin{aligned} E_{\mathrm{sca}}(\mathbf{r}) &\sim \frac{\omega\mu}{4} e^{j\pi/4} e^{-jkR} \sqrt{\frac{2}{\pi kR}} \\ &\sim \frac{\omega\mu}{4} H_0^{(2)}(kR) = -E_{\mathrm{inc}}(\mathbf{r}) \end{aligned} \tag{22}$$

with $R = [(x-x_0)^2 + z_0^2]^{1/2}$, which exactly cancels the incident field at any observation point x. At the higher-order branch points with $p \neq 0$ the current $\tilde{J}_0^{\infty}(k_x)$ in (20) behaves as

$$\tilde{J}_0^{\infty}(k_x) = A_p + B_p k_{z,p} + C_p k_{z,p}^2 + \cdots$$

where $A_p = -J_0(kw/2)/J_0(k_{b,p}w/2)$.

As shown in Appendix B, the higher-order asymptotic contribution arising from the B_0 term of (21) at the $k_x = k$ branch point, as well as the dominant contributions B_p from the other branch points in each pth region (see Fig. 3) provides a spatial wave that varies along the interface as

$$E_{\rm sp}(x) \sim \sum_{p=-\infty}^{\infty} b_p(z) B_p(\boldsymbol{r}_0) \frac{e^{-jk_{b,p}^{+}x}}{x^{3/2}} \tag{23}$$

with propagation wavenumbers $k_{b,p}^{+}$ for $p = 0, \pm 1, \pm 2, \ldots$ defined in (5), and b_p being coefficients that are defined in Appendix B. Hence, the space wave along the periodic artificial material interface decays algebraically as $x^{-3/2}$, and consists of an infinite number of space harmonics.

VII. Asymptotic Behavior of the Spatial Wave at the Interface

The properties observed above for the simple analytical canonical problem of the conducting strip grating are here generalized to structures as those in Fig. 1(a) and (b). For observation points sufficiently away from the source, and along the air interface of the periodic material, i.e., for $k|x + na - x'| \gg 1$, an asymptotic evaluation based on the steps reported in Appendix B is carried out for the general case involving the radiation integral in (15). To this end, the integral (15) is rewritten as

$$E_{\rm sca}(\mathbf{r} + na\hat{\mathbf{x}}, r_0) = \frac{-\omega\mu}{4\pi} \int_{-\infty}^{\infty} \frac{\mathrm{e}^{-j[(x+na)k_x + zk_z]}}{k_z} \cdot \tilde{J}_0^{\infty}(\mathbf{r}_0, k_x)\, dk_x \tag{24}$$

where $\tilde{J}_0^{\infty}(\mathbf{r}_0, k_x)$ is now the 2-D Fourier transform of the post current with transform variables (k_x, k_z), as defined in (29). In order to factorize the observer and the source terms in (24) it has been assumed for simplicity that the observation point $\mathbf{r}$ is slightly above the periodic material, i.e., $z \geq z'$ for all $z' \in S_0$. Once the definition of $\tilde{J}_0^{\infty}(\mathbf{r}_0, k_x)$ is used in (7) it is possible to observe that $\tilde{J}_0^{\infty}(\mathbf{r}_0, k_x) = -\mathrm{e}^{jk_x x_0}$ for $k_x = k$ (note that (21) assumes that $x_0 = 0$). This follows from substituting (3) into (7), multiplying both sides by k_z, and then taking the limit as k_z approaches k. The branch points at $k_x = k_{b,p}^{\pm}$ [see (5)] appear in the higher-order expansion terms of $\tilde{J}_0^{\infty}(\mathbf{r}_0, k_x)$ near $k_x = k_{b,p}^{\pm}$, as already seen for the strip grating case. By using the same argument as in Section III, once the incident field is included in (24), an expansion of the total field becomes (assuming here that $z \geq z_0$)

$$E_{\rm tot}(\mathbf{r} + na\hat{\mathbf{x}}, \mathbf{r}_0) = \frac{-\omega\mu}{4\pi} \int_{-\infty}^{\infty} \frac{\mathrm{e}^{-j[(x+na)k_x + zk_z]}}{k_z} \cdot \left[\tilde{J}_0^{\infty}(\mathbf{r}_0, k_x) + \mathrm{e}^{j[x_0 k_x + z_0 k_z]}\right] dk_x. \tag{25}$$

An asymptotic evaluation of the integral is carried out by deforming the original integration path along the real k_x axis onto the infinite number of vertical path contributions $C_{b,p}$ shown in Fig. 3. In the case that the source and observation points have approximately the same z-coordinate, i.e., $|z - z_0| \ll |x + na - x_0|$, and $|z - z'| \ll |x + na - x'|$, the paths $C_{b,p}$ coincide with the steepest-descent paths passing through $k_{b,p}^{+}$. Note that asymptotically, the dominant contribution at $k_{b,0}^{+} \equiv k$ vanishes because $\tilde{J}_0(\mathbf{r}_0, k_x) = -\mathrm{e}^{jk_x x_0}$. An asymptotic evaluation of the higher order term at $k_{b,0}^{+} = k$ and of the dominant contributions at $k_{b,p}^{+}$, with $p \neq 0$, as shown in Appendix B leads to a general representation of the spatial field in terms of an infinite number of space harmonics with a spreading factor $1/(x)^{3/2}$ as in (23), where the propagation wavenumbers $k_{b,p}^{+}$ are given in (5). Thus, the general form of the spatial field excited by a line source over a general periodic structure is observed to be the same as (23) for the canonical strip grating structure. In summary, from this asymptotic evaluation it is clear that the spatial field contribution in $E_{\rm tot}$ and $E_{\rm sca}$ decays as $1/x^{3/2}$ and $1/x^{1/2}$, respectively.

This is evidently the first time that such a conclusion has been reached for a line source over a general periodic structure. This property is expected to be relevant for the estimation of the coupling between two sources near a 1-D periodic artificial material. The conclusion should remain valid as the period tends to zero, in which case the periodic artificial material slab approaches a homogeneous artificial slab (e.g., a metamaterial slab with a negative permittivity).

VIII. Numerical Examples

A first example is shown in Figs. 4–6, where an electric line source is placed over an artificial material EBG slab consisting of three layers of periodic conducting cylinders with normalized radius $r/a = 0.2$ in free space. The axes of the cylinders in the first row are located at $z = 0$. The source is located at $\mathbf{r}_0 \equiv (x_0, z_0) = (0, 0.5)a$. In the MoM calculations each cylinder has been discretized using 16 sub-domain pulse basis functions. In Fig. 4, the operating frequency corresponds to $a/\lambda = 0.3$ and is thus in the 0th band gap $(0 < a/\lambda < 0.48)$ of the infinite EBG material [18]. The total field $E_{\rm tot}$ (normalized by multiplying with the period a) is plotted versus the distance na from the line source parallel to the EBG interface, at points $\mathbf{r}_{A,n} = na\hat{\mathbf{x}} + a\hat{\mathbf{z}}$ and $\mathbf{r}_{B,n} = (0.5 + n)a\hat{\mathbf{x}} + 0.5a\hat{\mathbf{z}}$, with n denoting the supercell index. The total field is obtained by adding the scattered field in (9) to the incident field. In Fig. 4, it is seen that the total field is dominated by the space wave, and exhibits the expected algebraic decay $1/n^{3/2}$ of the space wave at both observer locations. (The $1/n^{3/2}$ curves are normalized to the exact curves for large n.) This indicates the absence of guided modes for this structure at this particular frequency.

In Fig. 5, the field is evaluated along the interface for various frequencies, and the decay is compared with the algebraic decay $1/n^{3/2}$ normalized to the exact fields for large n. These numerical experiments indicate that the field at large distance behaves like

$$E_{\rm tot}(\mathbf{r} + na\hat{\mathbf{x}}, \mathbf{r}_0) \sim w(\mathbf{r}, \mathbf{r}_0) \frac{e^{-jkna}}{n^{3/2}} \tag{26}$$

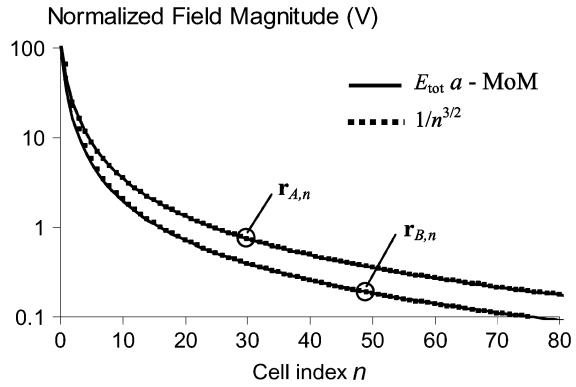

Fig. 4. Spatial decay of the total field produced by a line source over the periodic EBG material of Fig. 1(a) made of 3 layers of periodic conducting cylinders. The field is evaluated at points $\mathbf{r}_{A,n}$ and $\mathbf{r}_{\mathrm{B},n}$ where n denotes the supercell index. The fields match well with a simple $1/n^{3/2}$ factor (normalized to the exact fields for large n).

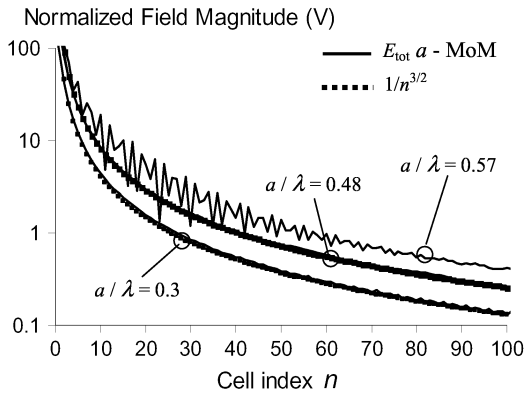

Fig. 5. For the same geometry of Fig. 4, the field is evaluated at points $\mathbf{r}_{A,n}$, where n denotes the supercell index, for various frequencies. The fields match well with a simple $1/n^{3/2}$ factor (which is normalized to the exact fields for large n) for the two lower frequencies.

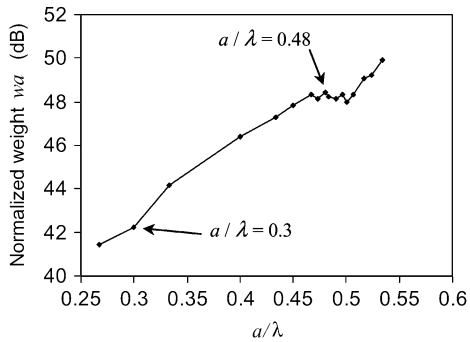

Fig. 6. For the same geometry of Fig. 5, the normalized weighting coefficient $aw(\mathbf{r}, \mathbf{r}_0)$ (in decibels relative to 1 V) of the space wave is plotted versus normalized frequency.

where $\mathbf{r}$ denotes the observation point within the $n = 0$ supercell. The weights $w(\mathbf{r}, \mathbf{r}_0)$ are reported for various frequencies in Fig. 6. Although the weight expression

$$w(\mathbf{r}, \mathbf{r}_0) = \sum_{p=-\infty}^{\infty} b_p(z) B_p(\mathbf{r}_0) e^{-jk_{b,p}^{+} x} \tag{27}$$

could be derived from (23), here it has been determined by simply matching the exact field with the fitting curve $1/n^{3/2}$ for large n.

Note that $a/\lambda = 0.48$ is at the edge of the passband [18] where the material approximately behave like an artificial material with a zero permittivity [19].

At higher frequencies, such as $a/\lambda = 0.567$, a leaky mode is propagating along the interface as can be seen from the interference between the space wave and the leaky wave in Fig. 5 (the interference subsides for larger distances, due to the exponential decay of the leaky mode). From a numerical search in the complex plane, it has been found that the wavenumber $\beta - \mathrm{j}\alpha$ of the leaky wave pole (corresponding to the pole location in the zeroth Brillouin zone) is approximately

$$\beta = 0.26k, \quad \alpha = 0.017k.$$

The above phase and attenuation constants correlate well with the "subtracted field" on the interface that is obtained after the asymptotic spatial field is subtracted from the total field (the results are omitted here). The subtracted field exhibits an exponential decay, as expected. As before, the spatial field decays as $1/n^{3/2}$.

As a second example, in Fig. 7 the total field is evaluated along the interface of the corrugated structure shown in Fig. 1(b) with $h = 0.5$ cm, $a = 0.4$ cm, for various frequencies. The source is located at $(x, z) = (0, 0.2)$ cm and the field is observed along the interface at locations (in cm) $\mathbf{r}_n = (0.2 + na)\hat{\mathbf{x}} + 0.2\hat{\mathbf{z}}$. The MoM calculations are performed discretizing the unit-cell tooth into 10 subdomain pulse basis functions and using image theory to account for the ground plane. For this geometry the space wave once again exhibits the expected algebraic decay $1/n^{3/2}$ for all the frequencies examined. Note that at $f = 15$ GHz the teeth height h is a quarter-wavelength in free space, which is the condition to realize an artificially soft surface [3], [8]. The frequency $f = 37.5$ GHz is the cutoff frequency for the TE polarization analyzed here to propagate into the teeth region as a waveguide mode. At $f = 40.36$ GHz the teeth are such that $h = \lambda_g/4$ where λ_g is the wavelength of the fundamental TE polarized waveguide mode in the parallel plate waveguide with plate separation $a = 0.4$ cm.

These numerical experiments indicate that the field at large distance behaves like (26) with the weight $w(\mathbf{r}, \mathbf{r}_0)$ reported for various frequencies in Fig. 8. Expression (26) coincides with (23) when the spatial harmonics are summed. It is worth noting that for $f = 40.36$ GHz, the total radiated field still exhibits a $1/n^{3/2}$ spatial decay, in contrast to a $1/n^{1/2}$ decay expected at the interface between air and a PMC, due to the presence of the conducting teeth.

The above results also verify that for TE polarization, the corrugated structure does not support surface-wave (bound) guided modes. This can be explained by the fact that the interface acts as a capacitive reactance for frequencies below 40.36 GHz, so that modal propagation of surface-wave modes is prohibited. Also, above 37.5 GHz the periodicity is greater that a half wavelength, so that any guided mode would be a leaky mode. Hence, propagation of surface-wave modes is prohibited in all frequency regions.

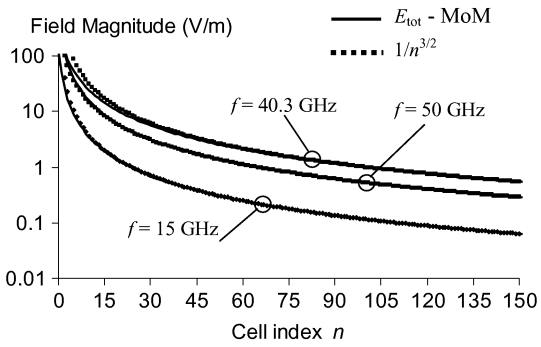

Fig. 7. Spatial decay of the total field produced by a line source over the corrugated surface shown in Fig. 1(b). The field is evaluated at points $\mathbf{r}_n$ where n denotes the supercell index. The field matches well with a simple $1/n^{3/2}$ factor (normalized to the exact fields for large n).

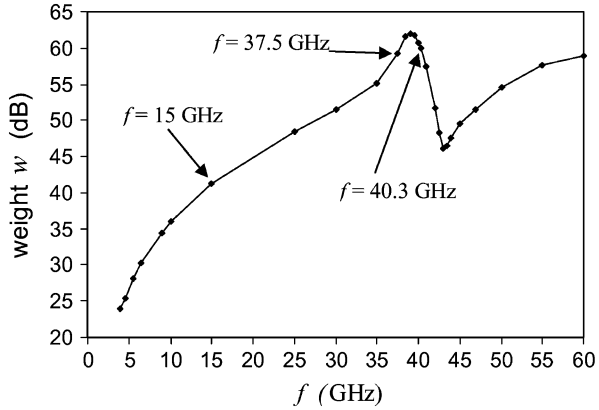

Fig. 8. Weighting coefficient $w(\mathbf{r}, \mathbf{r}_0)$ (in dB relative to 1 V/m) for the space wave representation in (26) versus frequency. Note that the amplitude of the space wave is maximum at approximately the frequency where the depth of the teeth is a quarter of wavelength for the fundamental TE mode of the corresponding parallel plate waveguide defined by the teeth.

IX. Conclusion

An efficient algorithm for the evaluation of the field produced by a line source near a periodic slab of artificial material has been derived using an "array-scanning method", which relates the field of a single line source to that produced by a periodic phased array of line sources. The complex wavenumber plane provides insight into the nature of the field produced. The main results from this study are as follows.

a) An efficient algorithm for the numerical evaluation of the field produced by a line source on top of the artificial material has been obtained.
b) The nature of the complex wavenumber plane and the periodic arrangement of the branch point singularities has been examined.
c) Based on the nature of the complex wavenumber plane, it was concluded that the space-wave field on the interface consists of an infinite number of space harmonics, each decaying algebraically as $x^{-3/2}$.
d) Guided modes (including leaky modes) may also be excited, if these are supported by the structure. The amplitudes of the Floquet waves that make up the guided mode are determined by the residues at the periodic pole locations in the complex wavenumber plane.
e) For a physical leaky mode, each pole in the periodic set is located on the lower sheet of the nearest pair of branch points, and on the top sheets of all others, when the mode radiates in the forward direction. When the mode radiates in the backward direction, the poles are located on the top sheet of all branch points. For a surface-wave mode, all of the poles are located on the top sheet of all branch points. (For the polarization and frequencies considered here, there were no surface-wave modes, however.)

The decay of the spatial wave has been demonstrated by numerical results, and also by an asymptotic analysis of a canonical problem consisting of a periodic conducting strip grating. This work lays the foundation for further studies involving other surfaces, including artificial magnetic conductors and other EBG materials. A formulation for 2-D periodic structures excited by a dipole source is also possible.

Appendix A
Determination of the Singularity Order

We determine here the order of the singularity of the integrand $E^{\infty}_{\rm sca}(\mathbf{r}, \mathbf{r}_0, k_x)$ in (9) at $k_x = k^{\pm}_{b,p}, p = 0, \pm 1, \pm 2, \ldots$ where $k^{\pm}_{b,p}$ is defined in (5). We first note that since $E^{\infty}_{\rm tot}(\mathbf{r}, \mathbf{r}_0, k_x) = 0$ for $\mathbf{r} \in S_0$, because of (10) $E^{\infty}_{\rm sca}(\mathbf{r}, \mathbf{r}_0, k_x)$ has the same singularities as $E^{\infty}_{\rm inc}(\mathbf{r}, \mathbf{r}_0, k_x)$ for $k_x = k^{\pm}_{b,p}$. Thus, $E^{\infty}_{\rm sca}(\mathbf{r}, \mathbf{r}_0, k_x)$ has a periodic set of singularities of the type $1/k_{zp} = 1/\sqrt{k^2 - k^2_{xp}}$ for $\mathbf{r} \in S_0$. It remains to demonstrate that $E^{\infty}_{\rm sca}(\mathbf{r}, \mathbf{r}_0, k_x)$ has also the same type of singularities for other observation points $\mathbf{r}$. To show this, for simplicity assume that the observation point $\mathbf{r}$ is slightly above the periodic material interface, i.e., $z \geq z'$ for all $z' \in S_0$. Then, substituting the explicit spectral form of the periodic Green's function (3) in (8) yields

$$E^{\infty}_{\rm sca}(\mathbf{r}, \mathbf{r}_0, k_x) = \frac{-\omega\mu}{4\pi} \sum_{p=-\infty}^{\infty} \frac{\mathrm{e}^{-j(k_{xp}x + k_{zp}z)}}{k_{zp}} \tilde{J}^{\infty}_p(\mathbf{r}_0, k_x) \tag{28}$$

with

$$\tilde{J}^{\infty}_p(\mathbf{r}_0, k_x) = \int_{S_0} \mathrm{e}^{+j(k_{xp}x' + k_{zp}z')} J^{\infty}_{S,\rm post}(\mathbf{r}', \mathbf{r}_0, k_x)\, d\mathbf{r}'. \tag{29}$$

Note that the terms $\tilde{J}^{\infty}_p(\mathbf{r}_0, k_x)$ do not depend on the observation point $\mathbf{r}$, and that the property

$$\tilde{J}^{\infty}_p\left(\mathbf{r}_0, k_x + \frac{2\pi}{a}p'\right) = \tilde{J}^{\infty}_{p+p'}(\mathbf{r}_0, k_x) \tag{30}$$

holds. Now, if for any point $\mathbf{r} \in S_0$ the singularity of $E^{\infty}_{\rm sca}(\mathbf{r}, \mathbf{r}_0, k_x)$ is $1/k_{zp}$, for a different $\mathbf{r}$, $\tilde{J}^{\infty}_p(\mathbf{r}_0, k_x)$ does not change and from (28) we infer that the singularity is still $1/k_{zp}$.

APPENDIX B
ASYMPTOTIC EVALUATIONS

In this Appendix, we provide the asymptotic evaluation of two important spectral integrals in order to determine the spatial behavior of the fields. Consider the form

$$I = \int_{-\infty}^{\infty} \frac{\mathrm{e}^{-jk_x X}}{k_z} \tilde{J}_0^{\infty}(k_x)\, dk_x = \sum_{p=-\infty}^{\infty} I_p \tag{31}$$

where $X = x + na - x'$ and $\tilde{J}_0^{\infty}(k_x)$ has branch points at $k_x = k_{b,p}^{\pm}$, with $p = 0, 1, 2, \ldots$ as given in (5) and shown in Fig. 3. The pth term denotes the integration along the p th steepest-descent path in Fig. 3. After the path deformation depicted in Fig. 3, the integral is represented as the sum of all the integration paths $C_{b,p}$ around the branch points (corresponding to the terms I_p). The asymptotic evaluation is first performed for the contribution of the path at the branch $k_x = k$, with $p = 0$, that renders $k_{z,0} = k_z = 0$. At this branch point,

$$\tilde{J}_0^{\infty}(k_x) = -\mathrm{e}^{jk_x x_0} + A_0 k_z + B_0 k_z^2 + \cdots,$$

and the integral I_0 in (31) is written as

$$\begin{aligned} I_0 &\sim \int_{C_{b,0}} \frac{\mathrm{e}^{-jk_x X}}{k_z} \left[-\mathrm{e}^{jk_x x_0} + A_0 k_z + B_0 k_z^2\right] dk_x \\ &= -\mathrm{e}^{jk_x x_0} \int_{C_{b,0}} \frac{\mathrm{e}^{-jk_x X}}{k_z}\, dk_x + B_0 \int_{C_{b,0}} k_z \mathrm{e}^{-jk_x X}\, dk_x. \end{aligned} \tag{32}$$

The term with A_0 vanishes, for it does not possess a branch point and the two parts of the corresponding vertical steepest descent path cancel. Asymptotically the integral I_0 is further reduced using $k_x \approx k$ as

$$\begin{aligned} I_0 \sim \frac{-\mathrm{e}^{jk_x x_0}}{\sqrt{2k}} &\int_{C_{b,0}} \frac{\mathrm{e}^{-jk_x X}}{\sqrt{k - k_x}}\, dk_x \\ &+ B_0 \sqrt{2k} \int_{C_{b,0}} \sqrt{k - k_x} \mathrm{e}^{-jk_x X}\, dk_x. \end{aligned} \tag{33}$$

The root assumes opposite values on the integration path in the top and bottom Riemann sheets. Next, the change of variables $k_x = k - jks^2$, with $dk_x = -jk2sds$ is applied and I_0 is rewritten as

$$\begin{aligned} I_0 \sim -\sqrt{2}\mathrm{e}^{-j\pi/4}\mathrm{e}^{-jkX} \Bigg(&\mathrm{e}^{jk_x x_0} \int_0^{\infty} \mathrm{e}^{-kXs^2}\, ds \\ &+ B_0 2jk^2 \int_0^{\infty} s^2 \mathrm{e}^{-kXs^2}\, ds \Bigg) \end{aligned} \tag{34}$$

where $\sqrt{k - k_x} = \exp(-j\pi/4)\sqrt{k}s$ has been used for the top Riemann sheet. Therefore, I_0 is evaluated asymptotically as

$$I_0 \sim -\frac{\sqrt{\pi}}{\sqrt{2k}} \mathrm{e}^{-j\pi/4} \mathrm{e}^{-jkX} \left(\frac{\mathrm{e}^{jk_x x_0}}{\sqrt{X}} + jB_0 \frac{k}{X^{3/2}} \right). \tag{35}$$

It follows, therefore, that for $p = 0$ the constant in (23) is

$$b_0 = -j \frac{\sqrt{\pi k}}{\sqrt{2}} \mathrm{e}^{-j\pi/4} \left(\frac{-\omega\mu}{4\pi} \right).$$

At any other $p \neq 0$ branch point, the integrand in (31) is approximated as $\tilde{J}_0^{\infty}(k_x) = A_p + B_p k_{z,p} + C_p k_{z,p}^2 + \cdots$ and the corresponding I_p in (31) reduces to

$$\begin{aligned} I_p &\sim \int_{C_{b,p}} \frac{\mathrm{e}^{-jk_x X}}{k_{z,0}} \left[B_p k_{z,p} + C_p k_{z,p}^2\right] dk_x \\ &\sim B_p \int_{C_{b,p}} \frac{k_{z,p}}{k_{z,0}} \mathrm{e}^{-jk_x X}\, dk_x. \end{aligned} \tag{36}$$

(The A_p term does not contribute since the two contributions from the top and bottom surfaces of the pth branch point cancel.) Asymptotically the integral I_p is further reduced as

$$I_p \sim B_p \frac{\sqrt{2k}}{\sqrt{k^2 - (k_{b,p}^{+})^2}} \int_{C_{b,p}} \sqrt{k_{b,p}^{+} - k_x} \mathrm{e}^{-jk_x X}\, dk_x. \tag{37}$$

The root inside the integral assumes opposite values on the integration path in the top and bottom Riemann sheets. Next, the change of variable $k_x = k_{b,p}^{+} - jk_{b,p}^{+} s^2$, with $dk_x = -jk_{b,p}^{+} 2sds$ is applied and I_p is rewritten as

$$I_p \sim B_p \frac{-2j\sqrt{2kk_{b,p}^{+}}}{\sqrt{k^2 - (k_{b,p}^{+})^2}} \mathrm{e}^{-j\pi/4} \mathrm{e}^{-jk_{b,p}^{+} X} \int_0^{\infty} s^2 \mathrm{e}^{-(k_{b,p}^{+} X)s^2}\, dk_x \tag{38}$$

where $\sqrt{k_{b,p}^{+} - k_x} = \exp(-j\pi/4)\sqrt{k_{b,p}^{+}}s$ has been used on the top Riemann sheet. The remaining integral in (38) is evaluated exactly leading to

$$I_p \sim B_p \frac{-\mathrm{e}^{j\pi/4}\sqrt{\pi k}}{\sqrt{2}\sqrt{k^2 - (k_{b,p}^{+})^2}} \frac{\mathrm{e}^{-jk_{b,p}^{+} X}}{k_{b,p}^{+} X^{3/2}}. \tag{39}$$

It follows, therefore, that for $p \neq 0$ the constants in (23) are

$$b_p = \frac{-\mathrm{e}^{j\pi/4}\sqrt{\pi k}}{\sqrt{2}\sqrt{k^2 - (k_{b,p}^{+})^2}} \frac{1}{k_{b,p}^{+}} \left(\frac{-\omega\mu}{4\pi} \right).$$

REFERENCES

[1] E. Yablonovitch, "Inhibited spontaneous emission in solid state physics and electronics," *Phy. Rev. Lett.*, vol. 55, pp. 2059–2062, 1987.

[2] D. Sievenpiper, L. Zhang, R. Broas, N. Alexopoulos, and E. Yablonovitch, "High-impedance electromagnetic surfaces with a forbidden frequency band," *IEEE Trans. Microw. Theory Tech.*, vol. 47, no. 11, pp. 2059–2074, Nov. 1999.

[3] P.-S. Kildal, "Artificially soft and hard surfaces in electromagnetics," *IEEE Trans. Antennas Propag.*, vol. 38, no. 10, pp. 1537–1544, Oct. 1990.

[4] H. Y. D. Yang, R. Kim, and D. R. Jackson, "Design considerations for modeless integrated circuit substrates using planar periodic patches," *IEEE Trans. Microw. Theory Tech.*, vol. 48, no. 12, pp. 2233–2239, Dec. 2000.

[5] R. Gonzalo, P. de Maagt, and M. Sorolla, "Enhanced patch-antenna performance by suppressing surface waves using photonic-bandgap substrates," *IEEE Trans. Antennas Propag.*, vol. 47, no. 11, pp. 2131–2138, Nov. 1999.

[6] T. Zhao, D. R. Jackson, and J. T. Williams, "Radiation characteristics of a 2D periodic slot leaky-wave antenna," in *Proc. IEEE AP-S/URSI Int. Symp., AP-S Digest*, San Antonio, TX, Jun. 16–21, 2002, pp. 482–485.

[7] S. Enoch, G. Tayeb, P. Sabouroux, N. Guérin, and P. Vincent, "A metamaterial for directive emission," *Phy. Rev. Lett.*, vol. 89, no. 21, Nov. 2002.

[8] Z. Ying and P.-S. Kildal, "Improvements of dipole, helix, spiral, microstrip patch and aperture antennas with ground planes by using corrugated soft surfaces," in *Proc. Inst. Elect. Eng. Proceedings, Microwaves, Antennas and Propagation*, vol. 143, Jun. 1996, pp. 244–248.
[9] R. B. Hwang and S. T. Peng, "Surface-wave suppression of resonance-type periodic structures," *IEEE Trans. Antennas Propag.*, vol. 51, no. 6, pp. 1221–1229, Jun. 2003.
[10] H. Y. Yang and D. R. Jackson, "Theory of line-source radiation from a metal-strip grating dielectric-slab structure," *IEEE Trans. Antennas Propag.*, vol. 48, pp. 556–564, Apr. 2000.
[11] B. A. Munk and G. A. Burrell, "Plane-wave expansion for arrays of arbitrarily oriented piecewise linear elements and its application in determining the impedance of a single linear antenna in a lossy half-space," *IEEE Trans. Antennas Propag.*, vol. 27, pp. 331–343, May 1979.
[12] C. P. Wu and V. Galindo, "Properties of a phased array of rectangular waveguides with thin walls," *IEEE Trans. Antennas Propagat.*, vol. 14, pp. 163–173, Mar. 1966.
[13] F. Capolino, D. R. Wilton, and W. A. Johnson, "Efficient computation of the 2D Green's function for 1D periodic layered structures using the Ewald method," *IEEE Trans. Antennas Propagat.*, 2005, to be published.
[14] A. W. Mathis and A. F. Peterson, "A comparison of acceleration procedures for the two-dimensional periodic Green's function," *IEEE Trans. Antennas Propagat.*, vol. 44, no. 4, pp. 567–571, Apr. 1996.
[15] F. Capolino, D. R. Jackson, and D. R. Wilton, "Numerical evaluation and field representation in 2D periodic artificial materials excited by a line source," in *Proc. ICEAA Int. Conf. Electromagnetics and Advanced Appl.*, Torino, Italy, Sep. 8–12, 2003, pp. 651–654.
[16] R. Sigelmann and A. Ishimaru, "Radiation from periodic structures excited by an aperiodic source," *IEEE Trans. Antennas Propagat.*, vol. 13, no. 3, pp. 354–364, May 1965.
[17] F. Capolino and M. Albani, "Scattering by truncated arrays of narrow strips: A Wiener–Hopf formulation," presented at the URSI-IEEE AP-S Symp., Boston, MA, Jul. 8–13, 2001.
[18] E. I. Smirnova, C. Chen, M. A. Shapiro, J. R. Sirigiri, and R. J. Temkin, "Simulation of photonic band gaps in metal rod lattices for microwave applications," *J. Appl. Phys.*, vol. 91, no. 3, pp. 960–968, Feb. 1, 2002.
[19] P. A. Below, S. A. Tretyakov, and A. J. Viitanen, "Dispersion and reflection properties of artificial media formed by regular lattices of ideally conducting wires," *J. Electromagnetic Waves and Appl.*, vol. 16, no. 8, pp. 1153–1170, 2002.

Filippo Capolino (S'94–M'97–SM'04) was born in Florence, Italy, in 1967. He received the Laurea degree (*cum laude*) in electronic engineering and the Ph.D. degree from the University of Florence, Italy, in 1993 and 1997, respectively.

From 1994 to 2000, he was a Lecturer of antennas at the Diploma di Laurea, University of Siena, Italy, where he has been a Research Associate until 2002 and presently employed as an Assistant Professor. From 1997 to 1998, he was a Fulbright Research Visitor with the Department of Aerospace and Mechanical Engineering, Boston University, Boston, MA, where he continued his research with a Grant from the Italian National Council for Research (CNR), from 1998 to 1999. From 2000 to 2001, he was Research Assistant Visiting Professor with the Department of Electrical and Computer Engineering, University of Houston, Houston, TX, where he is now an Adjunct Assistant Professor. In November to December 2003, he was an Invited Assistant Professor at the Institut Fresnel, Marseille, France. His primary research interests is in high-frequency, short-pulse radiation, array antennas, periodic structures, and metamaterials. He is the coordinator of the Siena Unit for the Network of Excellence "Metamorphose" on Metamaterials of the EU FP6.

Dr. Capolino was awarded with a MMET'94 Student Paper Competition Award in 1994, the Raj Mittra Travel Grant for Young Scientists in 1996, the "Barzilai" prize for the best paper at the National Italian Congress of Electromagnetism (XI RiNEm) in 1996, and a Young Scientist Award for participating at the URSI Int. Symp. Electromagn. Theory in 1998. He received the R. W. P. King Prize Paper Award from the IEEE Antennas and Propagation Society for the Best Paper of the Year 2000, by an author under 36. He is an Associate Editor for the IEEE TRANSACTIONS OF ANTENNAS AND PROPAGATION.

David R. Jackson (S'83–M'84–SM'95–F'99) was born in St. Louis, MO, on March 28, 1957. He received the B.S.E.E. and M.S.E.E. degrees from the University of Missouri, Columbia, in 1979 and 1981, respectively, and the Ph.D. degree in electrical engineering from the University of California, Los Angeles, in 1985.

From 1985 to 1991, he was an Assistant Professor in the Department of Electrical and Computer Engineering at the University of Houston, Houston, TX. From 1991 to 1998, he was an Associate Professor in the same department, and since 1998, he has been a Professor in this department. His present research interests include microstrip antennas and circuits, leaky-wave antennas, leakage and radiation effects in microwave integrated circuits, periodic structures, and EMC.

Dr. Jackson is presently serving as the Chair of the Transnational Committee of the IEEE AP-S Society, and as the Vice Chair for URSI, U.S. Commission B. He is also on the Editorial Board for the IEEE TRANSACTIONS ON MICROWAVE THEORY AND TECHNIQUES. Previously, he has been the Chapter Activities Coordinator for the IEEE AP-S Society, a Distinguished Lecturer for the AP-S Society, an Associate Editor for the IEEE TRANSACTIONS ON ANTENNAS AND PROPAGATION, and a member of the AdCom for the AP-S Society. He has also served as an Associate Editor for the Journal Radio Science and the International Journal of RF and Microwave Computer-Aided Engineering.

Donald R. Wilton (S'63–M'65–SM'80–F'87) was born in Lawton, OK, October 25, 1942. He received the B.S., M.S., and Ph.D. degrees from the University of Illinois, Urbana-Champaign, in 1964, 1966, and 1970, respectively.

From 1965 to 1968, he was with Hughes Aircraft Co., Fullerton, CA, engaged in the analysis and design of phased array antennas. From 1970 to 1983, he was with the Department of Electrical Engineering, University of Mississippi, and since 1983, he has been Professor of Electrical Engineering at the University of Houston. From 1978 to 1979, he was a Visiting Professor at Syracuse University, Syracuse, NY. His primary research interest is in computational electromagnetics, and he has published, lectured, and consulted extensively in this area.

Dr. Wilton is a member of Commission B of URSI, and has served as Secretary (two terms), Technical Activities Committee Chair, Vice Chair, and Chair of U. S. Commission B. He has also served as a Member-at-Large of USNC/URSI. He is a Fellow of the IEEE and has served the IEEE Antennas and Propagation Society as an Associate Editor of the IEEE TRANSACTIONS ON ANTENNAS AND PROPAGATION, as a Distinguished National Lecturer, and as a member of AdCom. He received the IEEE Third Millennium Medal and the Distinguished Alumni Award from the ECE Department, University of Illinois. He currently serves as an Associate Editor of the IEEE Press *Series on Electromagnetics*.